Numerical Modeling of Water Pressure in Propagating Concrete Cracks

Omid Reza Barani[1]; Saleh Majidaie[2]; and Mohammadnabi Mosallanejad[3]

Abstract: Modeling of water flow in the propagating cracks plays an important role in the stability analysis of concrete dams. The water pressure within concrete cracks is a function of water permeability of the crack. In this paper, a partially saturated finite-element algorithm is used for numerical modeling of water pressure within a propagating cohesive crack. In order to calculate fracture opening along the crack path suitably, a trilinear cohesive law is considered to describe mechanical behavior of the fracture process zone. The zero-thickness cohesive interface elements are used to capture the mixed-mode fracture behavior in tension and compression. On the basis of the experimental data, it is shown that a unified formula for natural fractures permeability can suitably describe the permeability of a propagating crack in both cases of slow and fast loading rates. **DOI: 10.1061/(ASCE)EM.1943-7889.0001048.** © *2016 American Society of Civil Engineers.*

Author keywords: Crack permeability; Concrete; Partially saturated porous media; Cohesive fracture.

Introduction

Modeling of water flow in the propagating cracks plays an important role in the stability analysis of concrete dams. These structures normally have cracks in practical service caused by previous earthquakes, construction conditions, or temperature effects. For a concrete dam subjected to its probable maximum flood, the hydrostatic pressure acting inside the crack induces additional material damage and hence reduces the resistance against further cracking and increases the penetration of water that exerts uplift pressure (Zhu and Pekau 2007). The water pressure inside the cracks significantly reduces the structural resistance of the concrete gravity dams (Bhattacharjee and Leger 1995). Significant research efforts on modeling of fracturing in concrete dams have been made over the last three decades (Chappell and Ingrafea 1981; Dewey et al. 1994; Feng et al. 1996; Plizzari 1997; Barpi and Valente 2000; Javanmardi et al. 2005; Pekau and Zhu 2008; Shi et al. 2013). Most of the numerical studies use the discrete crack approach because it offers a physically consistent and numerically precise way to model discontinuity of the crack and uplift pressures within crack surfaces (Shi et al. 2003).

The water pressure within concrete cracks is a function of water permeability of the crack. Experimental studies (Brühwiler and Saoma 1995a, b) have shown that the static pressure inside a crack is a function of crack opening and that along the fracture process zone this pressure reduces from full reservoir pressure to zero. Reinhardt et al. (1998) showed that cracks with an opening of more than approximately 0.04 mm are more permeable than undamaged concrete. For smaller crack widths, the penetration behavior is similar to that of uncracked concrete. From the experimental results, Slowik and Saouma (2000) proposed an interface model considering crack fluid permeability as a function of crack opening displacements. However, they did not consider roughness of crack walls as a key parameter in crack permeability. Barani et al. (2011) and Barani and Khoei (2014) developed a numerical tool to model cohesive crack propagation in semisaturated porous media. They considered a bilinear cohesive law to model the mechanical behavior of the fracture process zone. However, the bilinear cohesive law cannot properly simulate the opening of a propagating crack in the concrete fracture process zone.

The aim of this paper is to show that Barton's et al. (1985) formula for the permeability of natural fractures can suitably describe the permeability of a propagating crack in both cases of slow and fast loading rates.

A partially saturated finite-element algorithm is used for the numerical modeling of water pressure within a propagating cohesive crack. To calculate fracture opening along the crack path suitably, a trilinear cohesive law is considered to describe the mechanical behavior of the fracture process zone. The zero-thickness cohesive interface elements are used to capture the mixed-mode fracture behavior in tension and compression. The experimental data provided by Slowik and Saouma (2000) are used to show that Barton's formula, which considers the effect of wall roughness on the permeability of natural fractures, can suitably describe the permeability of a propagating crack in both cases of slow and fast loading rates.

Finite-Element Formulation of Semisaturated Porous Media

The material behavior of concrete can be described within the framework of the theory of porous media first formulated by Biot (1941). The first numerical solution for the Biot's equations was made by Ghaboussi and Wilson (1973). Zienkiewicz et al. (1990) proposed a simple extension of a two-phase formulation to semisaturated problems, assuming that the air or gas present in the pores remains at atmospheric pressure. The coupled equations that consider the air and water phases in a porous medium have been given by Alonso et al. (1990) and Gawin and

[1]Assistant Professor, Dept. of Civil Engineering, K.N. Toosi Univ. of Technology, P.O. Box 15875-4416, 1996715433 Tehran, Iran (corresponding author). E-mail: barani@kntu.ac.ir

[2]Graduate Student, Dept. of Civil Engineering, K.N. Toosi Univ. of Technology, P.O. Box 15875-4416, 1996715433 Tehran, Iran.

[3]Graduate Student, Dept. of Civil Engineering, K.N. Toosi Univ. of Technology, P.O. Box 15875-4416, 1996715433 Tehran, Iran.

Note. This manuscript was submitted on June 27, 2015; approved on October 23, 2015; published online on January 13, 2016. Discussion period open until June 13, 2016; separate discussions must be submitted for individual papers. This paper is part of the ***Journal of Engineering Mechanics***, © ASCE, ISSN 0733-9399.

Schrefler (1996). However, because of the great complexity of three-phase models, extensive specially designed tests are required to determine the properties of the matrix-air-water mixture.

The effective stress is an essential concept to describe the deformation of solid skeleton in the theory of porous media. The effective stress σ'_{ij} can be defined by $\sigma'_{ij} = \sigma_{ij} + \alpha\delta_{ij}S_w p_w$, where δ_{ij} = Kronecker delta; σ_{ij} = total stress with positive value in tension; and p_w = water pressure with positive value in compression. In this relation, α = Biot coefficient, defined by $\alpha = 1 - K_T/K_s$, with K_T and K_s = bulk modulus of porous medium and solid particles, respectively. S_w = water saturation, defined as a function of the water pressure, i.e., $S_w = S_w(p_w)$.

The linear momentum balance for the mixture of solid-fluid phase can be written as

$$\sigma_{ij,j} + \rho b_i = 0 \tag{1}$$

where b_i = body force per unit mass; and ρ = density of total mixture, defined by $\rho = nS_w\rho_w + (1-n)\rho_s$, with ρ_w = water density, ρ_s = density of solid particles, and n = porosity.

Incorporating the Darcy law, the mass balance for the fluid phase can be written as

$$[-k_{rm}k_{ij}(p_{w,j} + \rho_w\ddot{u}_j - \rho_w b_j)]_{,i} + \alpha S_w\dot{\varepsilon}_{ii} + \frac{\dot{p}_w}{Q^*} = 0 \tag{2}$$

where ε_{ii} = total volumetric strain; k_{ij} = permeability tensor of the medium; k_{rm} = relative permeability of the matrix, which is a function of the water pressure, i.e., $k_{rm} = k_{rm}(p_w)$; and Q^* is defined as

$$\frac{1}{Q^*} = C_s + n\frac{S_w}{K_w} + (\alpha - n)\frac{S_w}{K_w}\left(S_w + \frac{C_s}{n}p_w\right) \tag{3}$$

where K_w = bulk modulus for liquid phase; and C_s = specific moisture content, defined as ndS_w/dp_w (Zienkiewicz et al. 1999).

The governing Eqs. (1) and (2) can be discretized for quasi-static problems in the absence of acceleration terms by using two sets of shape functions $\mathbf{N}_u$ and $\mathbf{N}_p$ for two variables u_i and p_w, defined as $\mathbf{u} = \mathbf{N}_u\bar{\mathbf{u}}$ and $p_w = \mathbf{N}_p\bar{p}_w$, on the basis of the standard Galerkin technique to transform these equations into a set of algebraic equations as

$$\mathbf{K}\bar{\mathbf{u}} - \mathbf{Q}\bar{p}_w = \mathbf{f}^{(1)} \tag{4}$$

$$\mathbf{Q}\dot{\bar{\mathbf{u}}} + \mathbf{H}\bar{p}_w + \mathbf{G}\dot{\bar{p}}_w = \mathbf{f}^{(2)} \tag{5}$$

where the stiffness matrix $\mathbf{K}$, the coupling matrix $\mathbf{Q}$, the permeability matrix $\mathbf{H}$, and the compressibility matrix $\mathbf{G}$ are defined as

$$\mathbf{K} = \int_\Omega \mathbf{B}^T\mathbf{D}\mathbf{B}d\Omega \qquad \mathbf{Q} = \int_\Omega \mathbf{B}^T S_w\alpha\mathbf{m}\mathbf{N}_p d\Omega$$
$$\mathbf{H} = \int_\Omega \nabla\mathbf{N}_p^T\mathbf{k}k_{rm}\nabla\mathbf{N}_p d\Omega \qquad \mathbf{G} = \int_\Omega \mathbf{N}_p^T\frac{1}{Q^*}\mathbf{N}_p d\Omega \tag{6}$$

and

$$\mathbf{f}^{(1)} = \int_\Omega \mathbf{N}_u^T\rho\mathbf{b}d\Omega + \int_{\Gamma_t}\mathbf{N}_u^T\bar{\mathbf{t}}d\Gamma$$
$$\mathbf{f}^{(2)} = -\int_\Omega \mathbf{N}_p^T\nabla^T(\mathbf{k}k_{rm}\rho_w\mathbf{b})d\Omega + \int_{\Gamma_q}\mathbf{N}_p^T\frac{q_w}{\rho_w}d\Gamma \tag{7}$$

where $\mathbf{B}$ = matrix relating the increments of strain and displacements; $\mathbf{D}$ = material property matrix of solid skeleton; and $\mathbf{m} = [1,1,0,1]^T$ (Khoei et al. 2006). In the aforementioned relations, Ω = domain of fluid and solid fields; Γ_t = external boundary for traction; Γ_q = external boundary for influx; and q_w = imposed flux on Γ_q. The permeability matrix $\mathbf{k}$ is defined as

$$\mathbf{k} = \begin{bmatrix} k_x & k_{xy} \\ k_{yx} & k_y \end{bmatrix} \tag{8}$$

where k_x and k_y = permeability coefficients in x- and y-directions, respectively; and k_{xy} and k_{yx} = zero when x and y are principal directions of the permeability matrix.

Because of ongoing hydration, concrete remains unsaturated even though it is stored under water (Gawin et al. 2006). On the basis of the pore network model, a relationship between the capillary pressure and the water saturation is proposed by van Genuchten (1980) as

$$S_w(p_w) = \left[1 + \left(\frac{p_w}{p_r}\right)^{1/(1-m)}\right]^{-m} \tag{9}$$

in which the reference pressure p_r and the coefficient m are defined on the basis of the experimental data obtained by Baroghel-Bouny et al. (1999) as $p_r = 18.6237$ MPa and $m = 0.4396$, respectively. The relative permeability is defined for soils by van Genuchten (1980) as

$$k_{rm}(S_w) = \sqrt{S_w}[1 - (1 - S_w^{1/m})^m]^2 \tag{10}$$

The applicability of aforementioned relation in modeling of moisture transport in unsaturated concrete is shown by Savage and Janssen (1997).

Mechanical Behavior of Fractured Media

Cohesive zone modeling has gained considerable attention over the last decade, as it represents a powerful yet efficient technique to describe the mechanical behavior of fractures in quasi-brittle materials. It was originally introduced by Barenblatt (1959) and Dugdale (1960). During the fracture process, the microcracking phenomenon near the crack tip consumes a part of the external energy introduced by the applied load. Generally, the crack surface is a tortuous path because of crack branching around aggregates. The microcracking density distribution at the fracture front may vary depending on the structure size, shape, and type of loading.

The first implementation of cohesive crack model in the finite-element method was performed by Hilleborg et al. (1976). They extended the concept of cohesive crack for concrete by proposing that the cohesive crack may be assumed to develop anywhere, even if no preexisting macrocrack is actually present, which is called the fictitious crack model. Xu and Needleman (1994) proposed a potential-based cohesive law in which cohesive elements are inserted into a finite-element mesh in advance. Although the model of Xu and Needleman has been widely used because of its easy implementation, it induces artificial compliance because of the elasticity of intrinsic cohesive law (Song et al. 2006). To alleviate this problem, Geubelle and Baylor (1998) and Espinosa and Zavattieri (2003) proposed the bilinear cohesive zone model to reduce the compliance by providing an adjustable initial slope in the cohesive law. A suitable fracture criterion for the mixed-mode fracture was proposed by Camacho and Ortiz (1996) and is widely used in literature: the quasi-static crack propagation in quasi-brittle materials by Song et al. (2006) and Khoei et al. (2009); the quasi-static crack propagation in saturated porous media by Simoni and Secchi (2003), Schrefler et al. (2006), and Secchi et al. (2007); the dynamic crack propagation in saturated porous media by Khoei et al. (2011); and crack propagation in semisaturated porous media by

J. Eng. Mech., 2016, 142(4): 04016011

Barani et al. (2011). Khoei et al. (2011) indicated that if the cohesive elements are inserted only on the crack path, then increasing the number of cohesive elements does not increase artificial compliance. Recently, Barani and Khoei (2014) extended the cohesive crack model to simulated three-dimensional crack in semisaturated porous media. To determine crack permeability on the basis of crack propagation tests, in which there is a strong coupling between fluid pressure and crack propagation, it is important to model fracture process zone properly. Thus, in the following section, trilinear modeling of cohesive law and its finite-element formulation are described.

Theoritical Aspects of the Trilinear Cohesive Law and Finite-Element Implementation

The mixed-mode cohesive fracture model involves the simultaneous activation of normal and tangential displacement discontinuity with respect to the crack and corresponding tractions. In this model, the effective traction t_e is resolved into the normal and tangential components, i.e., t_n and t_s, where $t_e = \sqrt{t_n^2 + t_s^2}$. Likewise, the effective displacement is defined by $\delta_e = \sqrt{\delta_n^2 + \delta_s^2}$, where δ_n and δ_s = normal displacement and shear sliding of fracture surfaces, respectively. The nondimensional effective displacement can be defined as $\lambda_e = \sqrt{(\delta_n/\delta_c)^2 + (\delta_s/\delta_c)^2}$, where δ_c = critical displacement where complete separation, i.e., zero traction, occurs. In Fig. 1, the trilinear cohesive law is shown in terms of the normalized effective traction and normalized effective displacement. The prepeak region represents the elastic part of the intrinsic cohesive law, whereas the softening portion after the peak load accounts for the damage occurring in the fracture process zone. The parameter λ_{cr} is a nondimensional displacement, which is defined to adjust the prepeak slope of the cohesive law, and is set to a small value to obtain more exact results. If $\lambda_e < \lambda_{cr}$, the normal and shear tractions are given as

$$t_n = \frac{\sigma_c}{\lambda_{cr}}\left(\frac{\delta_n}{\delta_c}\right) \qquad t_s = \frac{\sigma_c}{\lambda_{cr}}\left(\frac{\delta_s}{\delta_c}\right) \tag{11}$$

where σ_c = material strength. For bilinear cohesive law, if $\lambda_e > \lambda_{cr}$, the normal and shear tractions in the case of loading are given by

$$t_n = \frac{\sigma_c}{\lambda_e}\frac{1-\lambda_e}{1-\lambda_{cr}}\left(\frac{\delta_n}{\delta_c}\right) \qquad t_s = \frac{\sigma_c}{\lambda_e}\frac{1-\lambda_e}{1-\lambda_{cr}}\left(\frac{\delta_s}{\delta_c}\right) \tag{12}$$

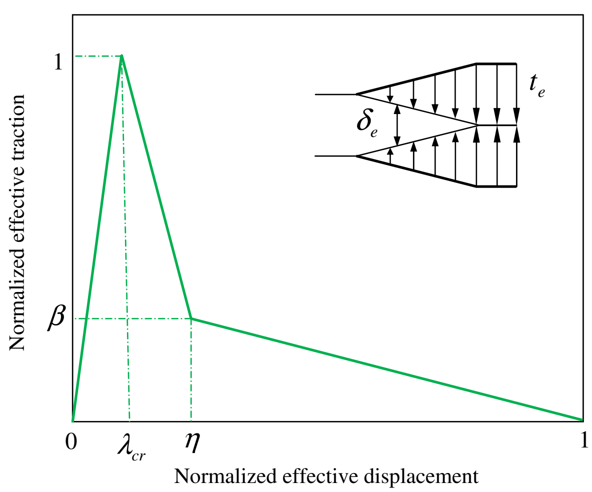

Fig. 1. Trilinear cohesive law in terms of normalized effective displacement and normalized effective traction

For trilinear cohesive law, if $\lambda_e > \lambda_{cr}$, the normal and shear tractions in the case of loading are given by

$$\begin{aligned} t_n &= \frac{\sigma_c}{\lambda_e}\left[\frac{\beta-1}{\eta-\lambda_{cr}}(\lambda_e-\lambda_{cr})+1\right]\left(\frac{\delta_n}{\delta_c}\right) \quad \lambda_{cr}<\lambda_e<\eta \\ t_s &= \frac{\sigma_c}{\lambda_e}\left[\frac{\beta-1}{\eta-\lambda_{cr}}(\lambda_e-\lambda_{cr})+1\right]\left(\frac{\delta_s}{\delta_c}\right) \end{aligned} \tag{13}$$

$$\begin{aligned} t_n &= \frac{\sigma_c}{\lambda_e}\frac{\beta}{1-\eta}(1-\lambda_e)\left(\frac{\delta_n}{\delta_c}\right) \quad \lambda_e>\eta \\ t_s &= \frac{\sigma_c}{\lambda_e}\frac{\beta}{1-\eta}(1-\lambda_e)\left(\frac{\delta_s}{\delta_c}\right) \end{aligned} \tag{14}$$

where β and η = ratio of breaking point strength to tensile strength and ratio of breaking point displacement to critical displacement, respectively (Fig. 1). In the case of unloading, the normal and shear tractions are given by

$$t_n = \frac{\sigma_c}{\lambda_{e1}}\frac{1-\lambda_{e1}}{1-\lambda_{cr}}\left(\frac{\delta_n}{\delta_c}\right) \qquad t_s = \frac{\sigma_c}{\lambda_{e1}}\frac{1-\lambda_{e1}}{1-\lambda_{cr}}\left(\frac{\delta_s}{\delta_c}\right) \tag{15}$$

where λ_{e1} = nondimensional displacement just before unloading. Fig. 2(a) shows the relation of t_n/σ_c and δ_n/δ_c with different values of δ_s/δ_c. Notice that in mixed mode, a cohesive law in terms of normalized opening displacement jump and normalized traction is not trilinear. The corresponding variations of t_s/σ_c and t_e/σ_c with δ_n/δ_c for different values of δ_s/δ_c are shown in Figs. 2(b and c), respectively. As shown in Fig. 2, for $\delta_s/\delta_c = 0$, the effective traction is equal to the normal traction. However, with increasing δ_s/δ_c, the value of t_n/σ_c decreases significantly.

To derive the components of cohesive material matrix $\mathbf{C}_f$ for the fractured zone, it needs to differentiate tractions with respect to the normal and shear displacements

$$\mathbf{C}_f = \begin{bmatrix} C_{ss} & C_{sn} \\ C_{ns} & C_{nn} \end{bmatrix} = \begin{bmatrix} \dfrac{\partial t_s}{\partial \delta_s} & \dfrac{\partial t_s}{\partial \delta_n} \\ \dfrac{\partial t_n}{\partial \delta_s} & \dfrac{\partial t_n}{\partial \delta_n} \end{bmatrix} \tag{16}$$

Hence, the components of cohesive material matrix $\mathbf{C}_f$ for $\lambda_e < \lambda_{cr}$ are governed by

$$C_{ss} = C_{nn} = \frac{\sigma_c}{\lambda_{cr}\delta_c}, \qquad C_{sn} = C_{ns} = 0 \tag{17}$$

For the trilinear cohesive law, the components of $\mathbf{C}_f$ matrix in the case of loading for $\lambda_{cr} < \lambda_e < \eta$ and $\lambda_e > \eta$ are given by

$$\begin{aligned} C_{ss} &= (\lambda_e-\lambda_{cr})\frac{\sigma_c\delta_c(\beta-1)}{\eta-\lambda_{cr}}\left(\frac{1}{\lambda_e\delta_c^2}-\frac{1}{\lambda_e^3}\frac{\delta_s^2}{\delta_c^4}\right) \\ &\quad + \frac{\sigma_c\delta_c(\beta-1)}{\eta-\lambda_{cr}}\left(\frac{\delta_s}{\lambda_e\delta_c^2}\right)^2 + \frac{\sigma_c}{\lambda_e\delta_c} - \frac{\sigma_c\delta_s^2}{\lambda_e^3\delta_c^3} \\ C_{sn} &= C_{ns} = \frac{\sigma_c}{\lambda_e^3\delta_c^3}\left[\frac{(\beta-1)}{\eta-\lambda_{cr}}\lambda_{cr}-1\right]\delta_s\delta_n \quad \lambda_{cr}<\lambda_e<\eta \end{aligned} \tag{18}$$

J. Eng. Mech., 2016, 142(4): 04016011

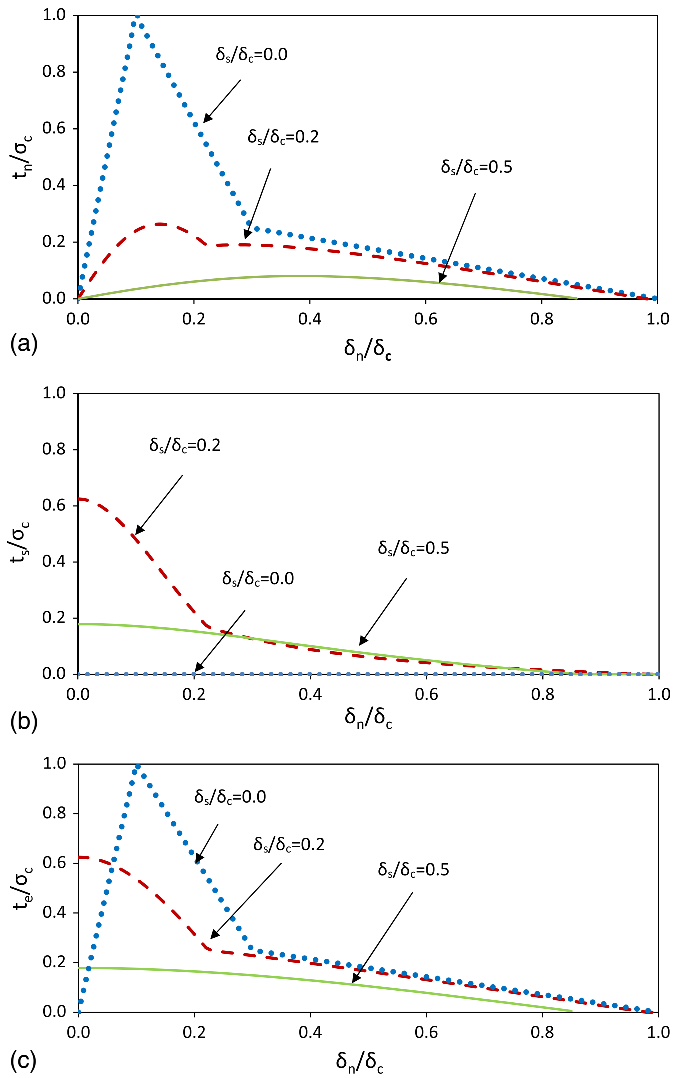

Fig. 2. (a) Relation of t_n/σ_c and δ_n/δ_c with different values of δ_s/δ_c; (b) corresponding variation of t_s/σ_c with δ_n/δ_c for different values of δ_s/δ_c; (c) corresponding variation of t_e/σ_c with δ_n/δ_c for different values of δ_s/δ_c

$$C_{nn} = (\lambda_e - \lambda_{cr})\frac{\sigma_c\delta_c(\beta-1)}{\eta-\lambda_{cr}}\left(\frac{1}{\lambda_e\delta_c^2} - \frac{1}{\lambda_e^3}\frac{\delta_n^2}{\delta_c^4}\right) + \frac{\sigma_c\delta_c(\beta-1)}{\eta-\lambda_{cr}}\left(\frac{\delta_n}{\lambda_e\delta_c^2}\right)^2 + \frac{\sigma_c}{\lambda_e\delta_c} - \frac{\sigma_c\delta_n^2}{\lambda_e^3\delta_c^3}$$

$$C_{ss} = (1-\lambda_e)\frac{\sigma_c\delta_c\beta}{1-\eta}\left(\frac{1}{\lambda_e\delta_c^2} - \frac{1}{\lambda_e^3}\frac{\delta_s^2}{\delta_c^4}\right) - \frac{\sigma_c\delta_c\beta}{1-\eta}\left(\frac{\delta_s}{\lambda_e\delta_c^2}\right)^2$$

$$C_{sn} = C_{ns} = -\frac{\sigma_c\delta_c\beta}{1-\eta}\frac{1}{\lambda_e^3}\left(\frac{\delta_s}{\delta_c^2}\right)\left(\frac{\delta_n}{\delta_c^2}\right) \qquad \lambda_e > \eta \tag{19}$$

$$C_{nn} = (1-\lambda_e)\frac{\sigma_c\delta_c\beta}{1-\eta}\left(\frac{1}{\lambda_e\delta_c^2} - \frac{1}{\lambda_e^3}\frac{\delta_n^2}{\delta_c^4}\right) - \frac{\sigma_c\delta_c\beta}{1-\eta}\left(\frac{\delta_n}{\lambda_e\delta_c^2}\right)^2$$

and in the case of unloading, they are given by

$$C_{ss} = C_{nn} = \frac{\sigma_c}{\delta_c}\left(\frac{1-\lambda_{e1}}{1-\lambda_{cr}}\right)\frac{1}{\lambda_{e1}}, \qquad C_{sn} = C_{ns} = 0 \tag{20}$$

If the normal component of traction is in compression, i.e., $t_n<0$ and $\delta_n = 0$, the cohesive shear traction t_{sC} can be defined according to Eqs. (1)–(5) as

$$t_{sC} = \frac{\sigma_c}{\lambda_{cr}}\left(\frac{\delta_s}{\delta_c}\right) \quad \text{if } \lambda_e<\lambda_{cr}$$

$$t_{sC} = \frac{\sigma_c}{\lambda_e}\left[\frac{\beta-1}{\eta-\lambda_{cr}}(\lambda_e-\lambda_{cr})+1\right]\left(\frac{\delta_s}{\delta_c}\right)$$

$$\text{if } \lambda_{cr}<\lambda_e<\eta \text{ (loading-trilinear)}$$

$$t_{sC} = \frac{\sigma_c}{\lambda_e}\frac{\beta}{1-\eta}(1-\lambda_e)\left(\frac{\delta_s}{\delta_c}\right)$$

$$\text{if } \lambda_e>\eta \text{ (loading-trilinear)}$$

$$t_{sC} = \frac{\sigma_c}{\lambda_{e1}}\frac{1-\lambda_{e1}}{1-\lambda_{cr}}\left(\frac{\delta_s}{\delta_c}\right) \quad \text{if } \lambda_e>\lambda_{cr} \text{ (unloading)} \tag{21}$$

and the nondimensional effective displacement is defined as $\lambda_e = |\delta_s/\delta_c|$. In this case, the shear traction can be computed by $|t_s| = |t_{sC}| + \mu|t_n|$, with μ = friction coefficient.

Finite-Element Formulation of Fractured Media

The formulation of this section is used to describe the hydro-mechanical behavior of fractured media including fracture process zone. The finite-element formulation of fractured media for quasi-static condition can be written similar to Eqs. (4) and (5) as

$$\mathbf{K}_f\bar{\mathbf{u}} - \mathbf{Q}_f\bar{p}_w = \mathbf{f}_f^{(1)} \tag{22}$$

$$\mathbf{Q}_f\dot{\bar{\mathbf{u}}} + \mathbf{H}_f\bar{p}_w + \mathbf{G}_f\dot{\bar{p}}_w = \mathbf{f}_f^{(2)} \tag{23}$$

where the cohesive stiffness matrix $\mathbf{K}_f$, the coupling matrix $\mathbf{Q}_f$, the permeability matrix $\mathbf{H}_f$, and the compressibility matrix $\mathbf{G}_f$ for the fractured zone are defined similar to the semisaturated porous media as

$$\mathbf{K}_f = \int_\Omega \mathbf{B}_f^T\mathbf{D}_f\mathbf{B}_f d\Omega$$

$$\mathbf{Q}_f = \int_\Omega \mathbf{B}_f^T S_w\mathbf{m}_f\mathbf{N}_f d\Omega$$

$$\mathbf{H}_f = \int_\Omega \nabla\mathbf{N}_f^T\mathbf{k}_f k_{rf}\nabla\mathbf{N}_f d\Omega$$

$$\mathbf{G}_f = \int_\Omega \mathbf{N}_f^T\frac{1}{Q_f^*}\mathbf{N}_f d\Omega$$

$$\mathbf{f}_f^{(1)} = \int_\Omega \mathbf{N}_f^T\rho_f\mathbf{b}d\Omega$$

$$\mathbf{f}_f^{(2)} = -\int_\Omega \mathbf{N}_f^T\nabla^T(\mathbf{k}_f k_{rf}\rho_w\mathbf{b})d\Omega \tag{24}$$

where $Q_f^* = 1/Q_f^* = nS_w/K_w$; $\rho_f = nS_w\rho_w$; k_{rf} = relative permeability of fractured zone; and $(k_f)_{ij}$ = fractured zone permeability tensor. In the aforementioned relations, $\mathbf{D}_f = w\mathbf{C}_f$, with w = fracture width; and the cohesive material matrix $\mathbf{C}_f$ is defined in Eq. (16).

The stiffness matrix of cohesive fracture elements can be obtained based on the standard contact elements (Khoei 2005). The relative displacements at any points along the fracture element, as shown in Fig. 3, are given by $\delta = \mathrm{u}_{\mathrm{top}} - \mathrm{u}_{\mathrm{bot}}$, where $\delta = \{\delta_s,\delta_n\}^T$; $\mathrm{u} = \{u_s,u_n\}^T$; $(u_s)_{\mathrm{top}}$ and $(u_n)_{\mathrm{top}}$ = displacements in the local s- and n-directions of the top side of the element, respectively; and $(u_s)_{\mathrm{bot}}$ and $(u_n)_{\mathrm{bot}}$ = displacements in the local s- and n-directions of the bottom side of the element, respectively. The relative displacements at any point of the element can be related to the nodal values by $\boldsymbol{\delta} = \mathbf{N}_f\bar{\mathbf{u}}$, with

J. Eng. Mech., 2016, 142(4): 04016011

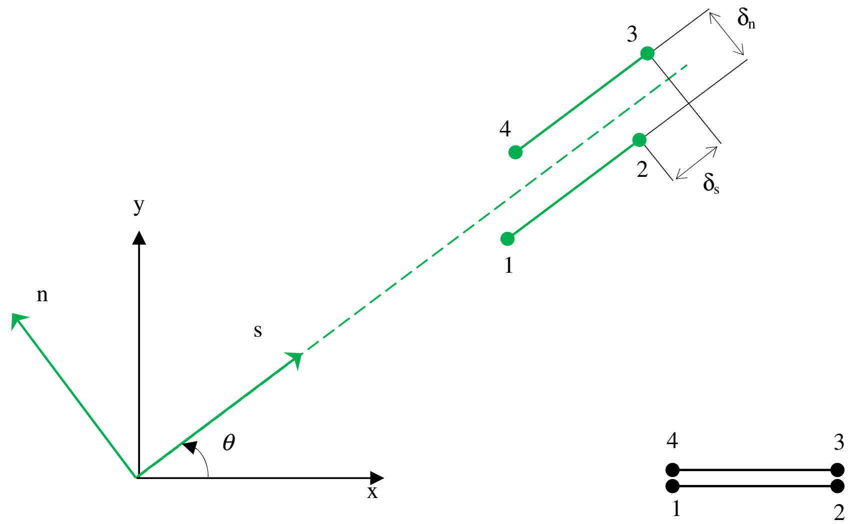

Fig. 3. Zero-thickness double-noded interface element

$\mathbf{N}_f = \langle -(\mathbf{N}_f)_{\mathrm{bot}}, (\mathbf{N}_f)_{\mathrm{top}} \rangle$ and $\bar{\mathbf{u}} = \langle \bar{\mathbf{u}}_{\mathrm{bot}}, \bar{\mathbf{u}}_{\mathrm{top}} \rangle^T$, where $\mathbf{N}_f$ = shape functions of cohesive fracture element, i.e., $(\mathbf{N}_f)_{\mathrm{bot}} = \{\mathbf{N}_{f1}, \mathbf{N}_{f2}\}$ and $(\mathbf{N}_f)_{\mathrm{top}} = \{\mathbf{N}_{f3}, \mathbf{N}_{f4}\}$. The shear and normal strains $\varepsilon = \{\gamma, \varepsilon_n\}$ are obtained from the relative displacements as $\gamma = (1/w)\delta_s$ and $\varepsilon_n = (1/w)\delta_n$. Hence, the strain vector can be defined as $\boldsymbol{\varepsilon} = \mathbf{B}_f \bar{\mathbf{u}}$, where the $\mathbf{B}_f$ matrix = $(1/w)\mathbf{N}_f$.

In Eq. (24), $\mathbf{m}_f = [1, 0, 1]^T$; $\nabla \mathbf{N}_f$ is defined as

$$\nabla \mathbf{N}_f = \begin{bmatrix} \frac{\partial N_{f1}}{\partial s} & \frac{\partial N_{f2}}{\partial s} & \frac{\partial N_{f3}}{\partial s} & \frac{\partial N_{f4}}{\partial s} \\ -\frac{N_{f1}}{w} & -\frac{N_{f2}}{w} & \frac{N_{f3}}{w} & \frac{N_{f4}}{w} \end{bmatrix} \quad (25)$$

and $\mathbf{k}_f$ is the fractured zone permeability matrix defined as

$$\mathbf{k}_f = \begin{bmatrix} k_l & 0 \\ 0 & k_n \end{bmatrix} \quad (26)$$

where k_l = longitudinal permeability coefficient; and k_n = transverse permeability coefficient. There are only a few published data available for water flow in semisaturated fractured zones, and the mechanism of flow and the characteristic behavior of relative permeability in fractured zones are still undetermined. Hence, in this study, the relative permeability of fractured zone is assumed to be $k_{rf} = 1$ according to (Meschke and Grasberger 2003). More

Table 1. Material Parameters for Concrete

Material properties	Fast loading	Slow loading
Elasticity modulus (MPa)	25,000	15,500
Poisson ratio	0.17	0.17
Density of solid particles (kg/m^3)	2,720	2,720
Water density (kg/m^3)	1,000	1,000
Bulk modulus of solid (MPa)	36,000	36,000
Bulk modulus of fluid (MPa)	3,000	3,000
Permeability (m^2/Pas)	10^{-15}	10^{-15}
Prosity	0.1	0.1
Fluid viscosity (MPa s)	10^{-9}	10^{-9}
Tensile strength (MPa)	1.6	1.6
Critical displacement δ_c (mm)	0.95	0.48
Ratio of breaking point strength to tensile strength	0.19	0.25
Ratio of breaking point displacement to critical displacement	0.085	0.148

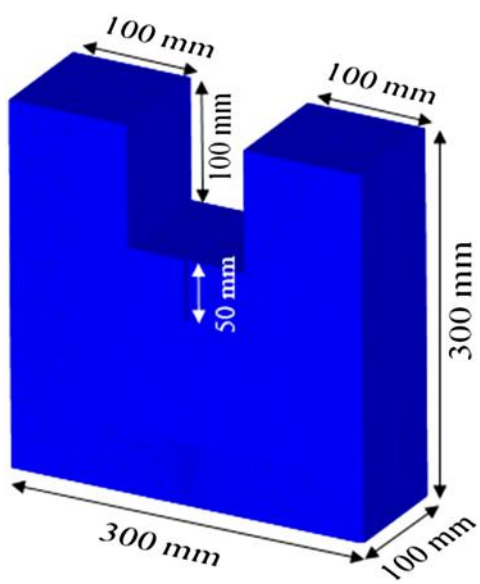

Fig. 4. Specimen geometry for wedge-splitting test

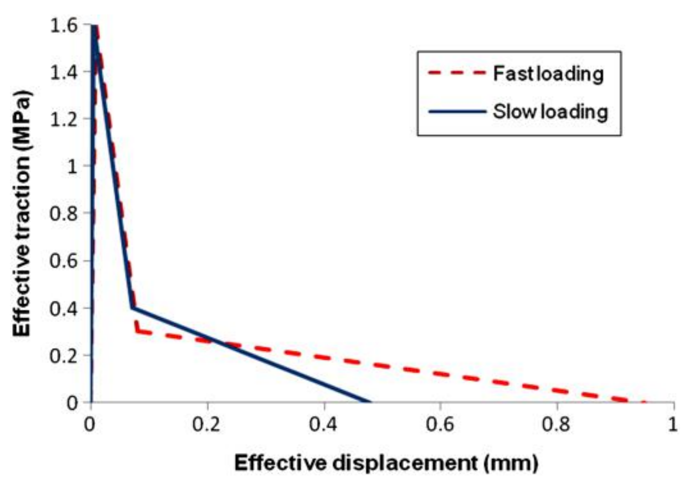

Fig. 5. Cohesive laws for both slow and fast loading rates

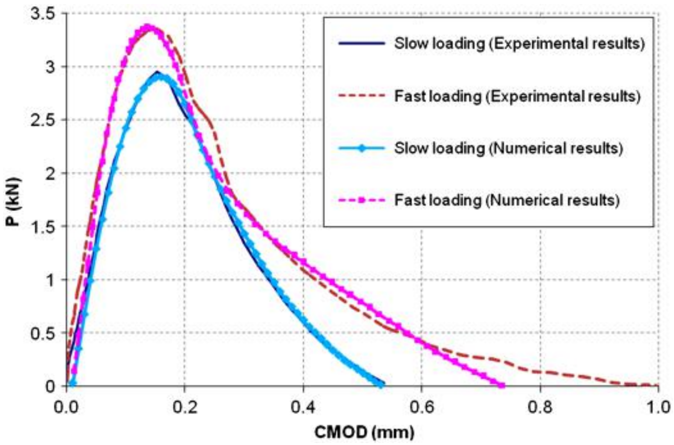

Fig. 6. Load versus CMOD for both experimental and numerical results of the slow and fast loading rates

details with regard to the numerical implementation can be found in Barani et al. (2011) and Khoei et al. (2011).

Assuming a large value for initial stiffness and transversal conductivity, the cohesive interface elements are inactive in both mechanical and fluid flow behavior before the stress reaches the tensile strength of the medium. Therefore, it is computationally convenient to use these elements on the crack path at the start of simulation. Furthermore, after the crack propagates and the cohesive tractions vanish, the stiffness of cohesive elements becomes zero, but their hydraulic behavior remains active.

Fractured Zone Permeability Coefficient

The parallel-plate model for fluid flow through a natural fracture is the only model for which an exact solution of the hydraulic conductivity is possible; this solution yields the well-known "cubic law" (Witherspoon et al. 1980). This model follows the assumption that the fracture walls can be represented by two smooth, parallel plates with infinite dimensions, separated by an aperture w. The real natural fractures and cracks, however, have finite sizes, rough walls, and variable apertures. Because of the roughness of the crack surfaces, the hydraulic conductivity of the natural fractures is much less than the theoretically estimated according to cubic law, and the parallel-plate model is inadequate to describe the flow in natural fractures (Sisavath et al. 2003).

For a natural fracture, the aperture can generally be defined as mechanical (geometrically measured) or hydraulic (measured by analysis of the fluid flow) (Olsson and Barton 2001). The mechanical fracture aperture w is defined as the average point-to-point distance between two fracture surfaces, perpendicular to the selected plane. Often, an average value is used to define the aperture. The hydraulic aperture e can be determined from the laboratory fluid-flow experiments. An important distinction has to be made between the theoretical smooth wall hydraulic aperture e and the real mechanical aperture w (geometrically measured) between two irregular fracture walls. Owing to the tortuosity and the wall

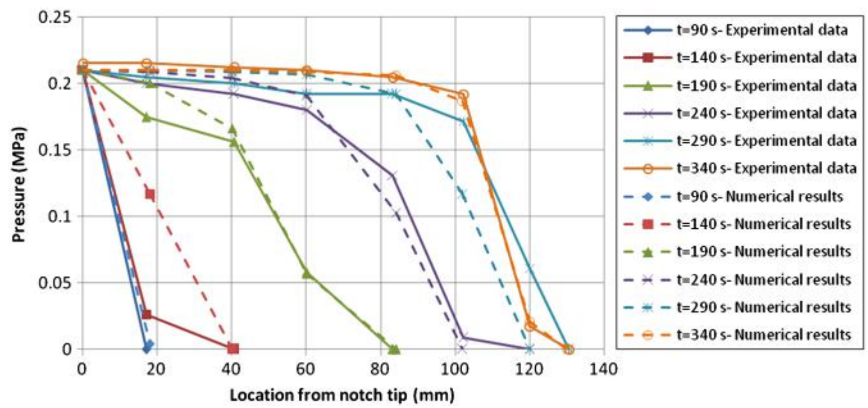

Fig. 7. Experimental and numerical water pressure variations for slow loading at various time steps using the input pressure of 0.21 MPa

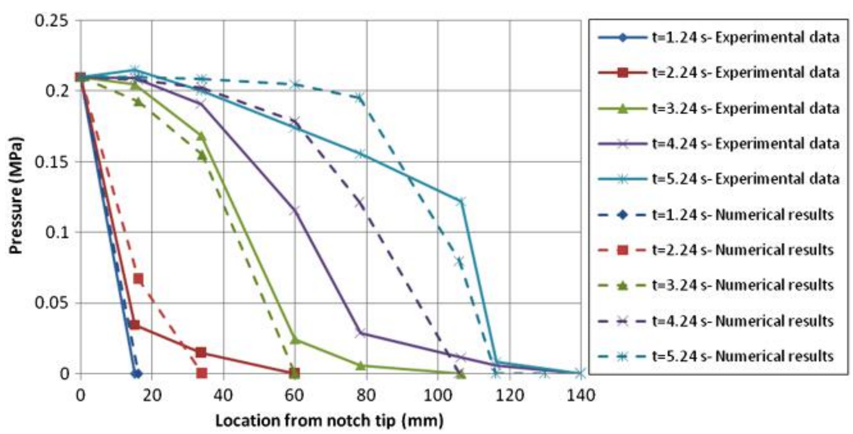

Fig. 8. Experimental and numerical water pressure variations for fast loading at various time steps using the input pressure of 0.21 MPa

friction, w is generally larger than e. An empirical model relating the hydraulic aperture e to the real mechanical aperture w and the fracture surfaces roughness JRC was proposed by Barton et al. (1985). This relationship was defined on the basis of the experimental data as

$$e = \frac{w^2}{JRC^{2.5}} \tag{27}$$

where e and w are expressed in micrometer. This equation is only valid for $w \geq e$. The roughness of the crack surface depends on the toughness and size of aggregates and the properties of matrix and interface. On the basis of the hydraulic aperture in the fractured zone, the longitudinal permeability coefficient k_l can be expressed as $e^2/12\mu$, where μ = dynamic viscosity.

Numerical Simulation Results

In this section, the proposed model for crack propagation in partially saturated porous media is applied to simulate experimental test results obtained by Slowik and Saouma (2000). They performed wedge-splitting tests with water pressure at the mouth of the crack to study water pressure inside the crack. The geometry of the specimen is presented in Fig. 4. The water input pressure is applied at the notch section, whereas zero pressure is assumed at the rest of the boundary. Two different rates are used for the crack-mouth opening displacement (CMOD), including the slow crack opening with the rate of 2 μm/s and the fast crack opening with the rate of 200 μm/s. The material properties used for experimental tests in the case of fast and slow loading rates are given in Table 1. Similar to Slowik and Saouma (2000), Barani et al. (2011) assumed the same elasticity modulus for both tests with fast and slow loading rates. However, this assumption cannot be verified with experimental results. In this study, elasticity modulus for fast loading test is assumed to be greater than for slow loading case. Fig. 5 shows the assumed effective traction–effective displacement relation for the fracture process zone in both fast and slow loading rate cases. As shown in this figure, the same tensile strength values are assumed in both cases, but the cohesive law in fast loading case has a longer tail. Fig. 6 presents the load versus CMOD for both experimental and numerical results of the slow and fast loading rates. As shown in this figure, very good agreement exists between numerical and experimental results, assuming trilinear cohesive law for concrete material. Figs. 7 and 8 present the experimental and numerical evolutions of water pressure along the crack path for different time steps at an input water pressure of 0.21 MPa for the slow and fast loading rates. Obviously, a good agreement can be observed between the experimental and numerical results. The results indicate that the Barton model with JRC equal to 20 satisfactorily predicts the hydraulic aperture for the entire of fractured zone.

Conclusion

In the present paper, a partially saturated finite-element algorithm was used for the numerical modeling of water pressure within a propagating cohesive crack. The behavior of fractured media was described by two equilibrium equations similar to those used for the mixture of solid-fluid phase in partially saturated media, including the momentum balance of fractured media and the balance of fluid mass within the fracture. To suitably calculate fracture opening along the crack path, a trilinear cohesive law was considered to describe the mechanical behavior of the fracture process zone. The zero-thickness cohesive interface elements were used to capture the mixed-mode fracture behavior in tension and compression. Finally, on the basis of the results of the wedge-splitting tests performed by Slowik and Saouma (2000), it has been shown that Barton's formula for permeability of natural fractures can suitably describe permeability of a propagating crack in both cases of slow and fast loading rates.

Acknowledgments

The financial support of the Iran National Science Foundation (INSF) under the Grant No. 91003668 is gratefully acknowledged.

References

Alonso, E. E., Gens, A., and Josa, A. (1990). "A constitutive model for partially saturated soils." *Geotechnique*, 40(3), 405–430.

Barani, O. R., and Khoei, A. R. (2014). "3D modeling of cohesive crack growth in partially saturated porous media: A parametric study." *Eng. Fract. Mech.*, 124–125, 272–286.

Barani, O. R., Khoei, A. R., and Mofid, M. (2011). "Modeling of cohesive crack growth in partially saturated porous media; a study on the permeability of cohesive fracture." *Int. J. Fract.*, 167(1), 15–31.

Barenblatt, G. I. (1959). "The formation of equilibrium cracks during brittle fracture: General ideas and hypotheses." *J. Appl. Math. Mech.*, 23(3), 622–636.

Baroghel-Bouny, V., Mainguy, M., Lassabatere, T., and Coussy, O. (1999). "Characterization and identification of equilibrium and transfer moisture properties for ordinary and high-performance cementitious materials." *Cem. Conc. Res.*, 29(8), 1225–1238.

Barpi, F., and Valente, S. (2000). "Numerical simulation of prenotched gravity dam models." *J. Eng. Mech.*, 10.1061/(ASCE)0733-9399(2000)126:6(611), 611–619.

Barton, N., Bandis, S., and Bakhtar, K. (1985). "Strength, deformation and conductivity coupling of rock joints." *Int. J. Rock. Mech. Min. Sci. Geomech. Abstr.*, 22(3), 121–140.

Bazant, Z. P., and Planas, J. (1998). *Fracture and size effect in concrete and other quasibrittle materials*, CRC Press, Boca Raton, FL.

Bhattacharjee, S. S., and Léger, P. (1994). "Application of NLFM models to predict cracking in concrete gravity dams." *J. Struct. Eng.*, 10.1061/(ASCE)0733-9445(1994)120:4(1255), 1255–1271.

Bhattacharjee, S. S., and Léger, P. (1995). "Fracture response of gravity dams due to rise of reservoir elevation." *J. Struct. Eng.*, 10.1061/(ASCE)0733-9445(1995)121:9(1298), 1298–1305.

Biot, M. A. (1941). "General theory of three dimensional consolidation." *J. Appl. Phys.*, 12(2), 155–164.

Brühwiler, E., and Saoma, V. E. (1995a). "Water fracture interaction in concrete. Part I: Fracture properties." *ACI Mater. J.*, 92(3), 296–303.

Brühwiler, E., and Saoma, V. E. (1995b). "Water fracture interaction in concrete. Part II: Hydrostatic pressure in cracks." *ACI Mater. J.*, 92(4), 383–390.

Camacho, G. T., and Ortiz, M. (1996). "Computational modeling of impact damage in brittle materials." *Int. J. Solids Struct.*, 33(2022), 2899–2938.

Chappell, J. F., and Ingraffea, A. R. (1981). "A fracture mechanics investigation of the cracking of Fontana Dam." *Dept. of Structural Engineering Rep. No. 81-7*, Cornell Univ., Ithaca, NY.

Dewey, R. R., Ronald, W. R., and Saouma, V. E. (1994). "Uplift modeling for fracture mechanics analysis of concrete dams." *J. Struct. Eng.*, 10.1061/(ASCE)0733-9445(1994)120:10(3025), 3025–3044.

Dugdale, D. S., (1960). "Yielding of steel sheets containing slits." *J. Mech. Phys. Solids*, 8(2), 100–104.

Espinosa, H. D., and Zavattieri, P. D. (2003). "A grain level model for the study of failure initiation and evolution in polycrystalline brittle materials. Part I: Theory and numerical implementation." *Mech. Mater.*, 35(3–6), 333–364.

Feng, L. M., Pekau, O. A., and Zhang, C. H. (1996). "Cracking analysis of arch dams by 3D boundary element method." *J. Struct. Eng.*, 10.1061/(ASCE)0733-9445(1996)122:6(691), 691–699.

Gawin, D., Pesavento, F., and Schrefler, B. A. (2006). "Hygro-thermo-chemo-mechanical modelling of concrete at early ages and beyond. Part I: Hydration and hygro-thermal phenomena." *Int. J. Numer. Methods. Eng.*, 67(3), 299–331.

Gawin, D., and Schrefler, B. A. (1996). "Thermo-hydro-mechanical analysis of partially saturated porous materials." *Eng. Comput.*, 13(7), 113–143.

Geubelle, P. H., and Baylor, J. (1998). "Impact-induced delamination of laminated composites: A 2D simulation." *Compos. Part B Eng.*, 29(5), 589–602.

Ghaboussi, J., and Wilson, E. L. (1973). "Flow of compressible fluid in porous elastic media." *Int. J. Numer. Methods Eng.*, 5(3), 419–442.

Hilleborg, A., Modeer, M. and Petersson, P. E. (1976). "Analysis of crack formation and crack growth in concrete by means of fracture mechanics and finite elements." *Cem. Concr. Res.*, 6(6), 773–781.

Javanmardi, F., Léger, P., and Tinawi, R. (2005). "Seismic water pressure in cracked concrete gravity dams: Experimental study and theoretical modeling." *J. Struct. Eng.*, 10.1061/(ASCE)0733-9445(2005)131:1(139), 139–150.

Khoei, A. R. (2005). *Computational plasticity in powder forming processes*, Elsevier, U.K.

Khoei, A. R., Barani, O. R., and Mofid, M. (2011). "Modeling of dynamic cohesive fracture propagation in porous saturated media." *Int. J. Numer. Anal. Methods Geomech.*, 35(10), 1160–1184.

Khoei, A. R., Gharehbaghi, S. A., Azami, A. R., and Tabarraie, A. R. (2006). "SUT-DAM: An integrated software environment for multi-disciplinary geotechnical engineering." *Advan. Eng. Software*, 37(11), 728–753.

Khoei, A. R., Moslemi, H., Majd Ardakany, K., Barani, O. R., and Azadi, H. (2009). "Modeling of cohesive crack growth using an adaptive mesh refinement via the modified-SPR technique." *Int. J. Fract.*, 159(1), 21–41.

Meschke, G., and Grasberger, S. (2003). "Numerical modeling of coupled hygromechanical degradation of cementitious materials." *J. Eng. Mech.*, 10.1061/(ASCE)0733-9399(2003)129:4(383), 383–392.

Olsson, R., and Barton, N. (2001). "An improved model for hydromechanical coupling during shearing of rock joints." *Int. J. Rock Mech. Mining Sci.*, 38(3), 317–329.

Pekau, O. and Zhu, X. (2008). "Effect of seismic uplift pressure on the behavior of concrete gravity dams with a penetrated crack." *J. Eng. Mech.*, 10.1061/(ASCE)0733-9399(2008)134:11(991), 991–999.

Plizzari, G. (1997). "LEFM applications to concrete gravity dams." *J. Eng. Mech.*, 10.1061/(ASCE)0733-9399(1997)123:8(808), 808–815.

Reinhardt, H. W., Sosoro, M., and Zhu, X. (1998). "Cracked and repaired concrete subject to fluid penetration." *Mat. Struct.*, 31(2), 74–83.

Savage, B. M., and Janssen, D. J. (1997). "Soil physics principles validated for use in predicting unsaturated moisture movement in portland cement concrete." *ACI Mater. J.*, 94(1), 63–70.

Schrefler, B. A., Secchi, S., and Simoni, L. (2006). "On adaptive refinement techniques in multi-field problems including cohesive fracture." *Comput. Methods Appl. Mech. Eng.*, 195(4-6), 444–461.

Secchi, S., Simoni, L., and Schrefler, B. A. (2007). "Mesh adaptation and transfer schemes for discrete fracture propagation in porous materials." *Int. J. Numer. Anal. Methods Geomech.*, 31(2), 331–345.

Shi, M., Zhong, H., Ooi, E., Zhang, C., and Song, C. (2013). "Modelling of crack propagation of gravity dams by scaled boundary polygons and cohesive crack model." *Int. J. Fract.*, 183(1), 29–48.

Shi, Z., Suzuki, M., and Nakano, M. (2003). "Numerical analysis of multiple discrete cracks in concrete dams using extended fictitious crack model." *J. Struct. Eng.*, 10.1061/(ASCE)0733-9445(2003)129:3(324), 324–336.

Simoni, L., and Secchi, S. (2003). "Cohesive fracture mechanics for a multi-phase porous medium." *Eng. Comput.*, 20(5/6), 675–698.

Sisavath, S., Al-Yaarubi, A., Pain, C., and Zimmerman, R. W. (2003). "A simple model for deviation from the cubic law for a fracture undergoing dilation or closure." *Pure Appl. Geophys.*, 160(5), 1009–1022.

Slowik, V., and Saouma, V. E. (2000). "Water pressure in propagating concrete cracks." *J. Struct. Eng.*, 10.1061/(ASCE)0733-9445(2000)126:2(235), 235–242.

Song, S. H., Paulino, G. H., and Buttlar, W. G. (2006). "A bilinear cohesive zone model tailored for fracture of asphalt concrete considering viscoelastic bulk material." *Eng. Fract. Mech.*, 73(18), 2829–2848.

van Genuchten, M. (1980). "A closed-form equation for predicting the hydraulic conductivity of unsaturated soil." *Soil Sci. Soc. Am. J.*, 44(5), 892–898.

Witherspoon, P. A., Wang, J. S. Y., Iwai, K., and Gale, J. E. (1980). "Validity of cubic low for fluid flow in a deformable rock fracture." *Water Resour. Res.*, 16(6), 1016–1024.

Xu, X. P., and Needleman, A. (1994). "Numerical simulations of fast crack growth in brittle solids." *J. Mech. Phys. Solids*, 42(9), 1397–1434.

Zhu, X., and Pekau, O. A. (2007). "Seismic behavior of concrete gravity dams with penetrated cracks and equivalent impact damping." *Engrg. Struct.*, 29(3), 336–345.

Zienkiewicz, O. C., Chan, A. H. C., Pastor, M., Schrefler, B. A., and Shiomi, T. (1999). *Computational geomechanics with special reference to earthquake engineering*, Wiley, New York.